# Aneuploidy Landscape in Precursors of Ovarian Cancer

Yeh Wang[1], Christopher Douville[2,3,4,5], Yen-Wei Chien[1], Brant G. Wang[6,7,8], Chi-Long Chen[9], Andre Pinto[10], Saron Ann Smith[11], Ronny Drapkin[12], M. Herman Chui[13], Tricia Numan[1,14], Russell Vang[1], Nickolas Papadopoulos[1,2,3,5], Tian-Li Wang[1,5,15], and Ie-Ming Shih[1,5,15]

## ABSTRACT

**Purpose:** Serous tubal intraepithelial carcinoma (STIC) is now recognized as the main precursor of ovarian high-grade serous carcinoma (HGSC). Other potential tubal lesions include p53 signatures and tubal intraepithelial lesions. We aimed to investigate the extent and pattern of aneuploidy in these epithelial lesions and HGSC to define the features that characterize stages of tumor initiation and progression.

**Experimental Design:** We applied RealSeqS to compare genome-wide aneuploidy patterns among the precursors, HGSC (cases, $n = 85$), and histologically unremarkable fallopian tube epithelium (HU-FTE; control, $n = 65$). On the basis of a discovery set ($n = 67$), we developed an aneuploidy-based algorithm, REAL-FAST (Repetitive Element AneupLoidy Sequencing Fallopian Tube Aneuploidy in STIC), to correlate the molecular data with pathology diagnoses. We validated the result in an independent validation set ($n = 83$) to determine its performance. We correlated the molecularly defined precursor subgroups with proliferative activity and histology.

**Results:** We found that nearly all p53 signatures lost the entire Chr17, offering a "two-hit" mechanism involving both *TP53* and *BRCA1* in *BRCA1* germline mutation carriers. Proliferatively active STICs harbor gains of 19q12 (*CCNE1*), 19q13.2, 8q24 (MYC), or 8q arm, whereas proliferatively dormant STICs show 22q loss. REAL-FAST classified HU-FTE and STICs into 5 clusters and identified a STIC subgroup harboring unique aneuploidy that is associated with increased proliferation and discohesive growth. On the basis of a validation set, REAL-FAST showed 95.8% sensitivity and 97.1% specificity in detecting STIC/HGSC.

**Conclusions:** Morphologically similar STICs are molecularly distinct. The REAL-FAST assay identifies a potentially "aggressive" STIC subgroup harboring unique DNA aneuploidy that is associated with increased cellular proliferation and discohesive growth. REAL-FAST offers a highly reproducible adjunct technique to assist the diagnosis of STIC lesions.

## Introduction

Ovarian high-grade serous carcinoma (HGSC) is a highly aggressive women's cancer and the fifth most common cause of female cancer–related death in the United States (1). Ovarian HGSC has long been thought to arise *de novo* from ovaries. However, a "crisis of confidence" for this assumption has surfaced in view of a dearth of evidence showing that HGSC precursors arise from the ovary *per se*. However, a wealth of clinicopathological, molecular genetic, epigenetic, transcriptomic, and proteomic evidence indicates that the majority of HGSCs originate from precursor lesions on the fallopian tube, known as serous tubal intraepithelial carcinomas (STIC; refs. 2–5). STICs are microscopic in size usually located on the surface of fallopian tube mucosa in the fimbriated ends. The STICs are characterized by a stretch of contiguous atypical epithelial cells showing several abnormal morphologic features (2, 6, 7). Another related lesion is the p53 signature, which contains a minute segment of fallopian tube epithelium (FTE) immunohistochemically showing intense p53 nuclear staining and harboring *TP53* missense mutations (8, 9). Interestingly, p53 signatures are morphologically indistinguishable from their adjacent non–*TP53*-mutated epithelium, indicating that *TP53* mutations alone are insufficient for transformation, and HGSC depends on other molecular genetic and epigenetic attributes. This new tubal paradigm of ovarian carcinogenesis posits that HGSC develops through precursor stages from normal-appearing FTE, p53 signature, and STIC. It serves as the biological basis for detecting HGSC in proximity fluids obtained from liquid Papanicolaou cervical samples and uterine lavage (4, 10, 11).

Some studies have proposed that tubal epithelial lesions may comprise distinct lesions showing some degree of histologic abnormalities and p53 immunostaining, but falling short for the diagnosis of STIC. Pathologists call them serous tubal intraepithelial lesions (STIL; ref. 12). Except for *TP53* mutations, there are few specific somatic mutations that are consistently associated with transitions from normal-appearing fallopian tubal epithelium to p53 signature and STIC (3, 13, 14). This may not come as a surprise, because among human neoplastic diseases, the proportion of the genome affected by copy-number changes (aneuploidy) far exceeds that affected by sequence changes (15). Aneuploidy refers to either gains or losses of entire chromosomes or subchromosomal regions. It is not only a result of chromosomal instability, but also plays a causal role in propelling tumor progression.

[1]Department of Pathology, Johns Hopkins Medical Institutions, Baltimore, Maryland. [2]Department of Oncology, the Sidney Kimmel Cancer Center, Johns Hopkins University School of Medicine, Baltimore, Maryland. [3]The Ludwig Center, Johns Hopkins University School of Medicine, Baltimore, Maryland. [4]The Sol Goldman Pancreatic Cancer Research Center, Johns Hopkins University School of Medicine, Baltimore, Maryland. [5]Sidney Kimmel Comprehensive Cancer Center, Johns Hopkins Medical Institutions, Baltimore, Maryland. [6]Department of Pathology, Inova Fairfax Hospital, Falls Church, Virginia. [7]School of Medicine Inova Campus, University of Virginia, Falls Church, Virginia. [8]Department of Pathology, Georgetown University Medical Center, Washington, DC. [9]Department of Pathology, College of Medicine, Taipei Medical University, Taipei, Taiwan. [10]University of Miami Sylvester Comprehensive Cancer Center, Miami, Florida. [11]Cascade Pathology Services, Legacy Health System, Portland, Oregon. [12]Department of Obstetrics and Gynecology and Basser Center for BRCA, University of Pennsylvania, Philadelphia, Pennsylvania. [13]Department of Pathology and Laboratory Medicine, Sloan-Kettering Cancer Center, New York, New York. [14]Department of Pathology, Sibley Memorial Hospital, Washington, DC. [15]Department of Gynecology and Obstetrics, Johns Hopkins Medical Institutions, Baltimore, Maryland.

Y. Wang and C. Douville contributed equally as co-authors of this article.

**Corresponding Authors:** Ie-Ming Shih, Johns Hopkins Medicine, 1550 Orleans Street, CRB2, Room 305-306, Baltimore, MD 21231. E-mail: ishih@jhmi.edu; Tian-Li Wang, tlw@jhmi.edu; and Christopher Douville, cdouvil1@jhmi.edu

Clin Cancer Res 2024;30:600–15

**doi:** 10.1158/1078-0432.CCR-23-0932

## Translational Relevance

There is growing evidence showing pelvic high-grade serous carcinoma (HGSC) develops from the fallopian tube epithelium through sequential stages of precursor lesions. A better understanding of these lesion species is critical in revealing the pathogenesis of HGSC and the development of improved diagnostic strategies. However, technical obstacles brought on by the diminutive size of these lesions, have made it challenging to conduct genome-wide molecular investigations. In this study, we applied RealSeqS, a sensitive PCR-based assay that can detect aneuploidy in samples containing pg of DNA, to assess the aneuploidy landscape in 138 microdissected tubal regions and 12 HGSCs. Our results showed that specific non-random aneuploidy patterns distinguish different types of precursor lesions, including a potentially "aggressive" STIC subtype that is associated with increased proliferation and discohesive growth. On the basis of the aneuploidy patterns, we developed an algorithm, Repetitive Element AneupLoidy Sequencing Fallopian Tube Aneuploidy in STIC (REAL-FAST) that promises a sensitive and specific molecular classification of heterogeneous STIC lesions.

Thanks to whole-exome and whole-genome sequencing, researchers have extensively assessed aneuploidy in a variety of human cancers, including their premalignant lesions (3, 16–21). However, these conventional methods face a technical challenge when the target lesions are extremely small, as in STIC and p53 signatures, which often have only a few hundred cells. We have recently developed a technique termed Repetitive Element AneupLoidy Sequencing System (RealSeqS), which uses a single-primer pair to amplify approximately 350,000 amplicons of repetitive elements across the genome (22, 23). RealSeqS is uniquely suitable for studying minimal quantities (sub-nanogram levels) of DNA from formalin-fixed and paraffin-embedded (FFPE) tissues.

The purpose of this study is to leverage RealSeqS to describe a comprehensive aneuploidy landscape in a relatively large number of precancerous lesions on fallopian tubes. The analysis of the RealSeqS data provides a basis for answering fundamental questions pertinent to the earliest events of HGSC development. In particular, we attempted to address whether all STICs are molecularly similar and, if not, whether there are aneuploidy patterns involving cancer driver genes that allow meaningful molecular classifications. We also used the MT-CO1 (cytochrome–c oxidase subunit 1) protein loss epithelium as a marker for control epithelium showing potential clonal origin (24–27). The answers are expected to help in the development of a diagnostic tool for detection of STICs and prediction of the clinical outcome in women with genetic predisposition.

# Materials and Methods

### Tissue samples and preparation

FFPE tissues were retrieved from the pathology archive at the Johns Hopkins Medical Institution (Baltimore, MD) and the Inova Fairfax Hospital (Fairfax, VA). This study was approved by an institutional review board and conducted in accordance with International Ethical Guidelines for Biomedical Research Involving Human Subjects (CIOMS). Because we used the archived FFPE tissues collected for prior clinical pathology diagnosis, the written informed consent was waived because the research would not be feasible or practicable to carry out without the waiver and poses no more than minimal risks to participants.

Before experiments, H&E (hematoxylin and eosin) slides and accompanying p53 and Ki-67–immunostained slides from all available cases were re-reviewed by at least two gynecologic pathologists (Y.-W. Chien, I.-M. Shih, and R. Vang) who arrived at a consensus diagnosis following the criteria previously reported (6). Proliferatively dormant STICs (hereafter "dormant STIC") or STIL, according to some investigators (6), were defined as STICs with Ki-67 labeling index, which is defined as the ratio (percentage) of positive cells over total cells counted, comparable with the background normal epithelia. Proliferatively active STICs (hereafter "active STICs") were defined as STICs with a Ki-67–labeling index more than 10%.

We performed laser capture-microdissection to enrich for epithelial cells of interest at 138 fallopian tube regions containing STIC lesions, p53 signatures, MT-CO1 protein loss epithelium, and randomly selected histologically unremarkable tubal epithelium (hereafter "NFTE"). The tissue samples were obtained from 61 women (Supplementary Table S1). Thirty-four STICs were incidental lesions (19 proliferatively active and 15 proliferatively dormant STICs), as they were not associated with concurrent HGSCs. Among STIC lesions, 37 were used as the training set to establish the REAL-FAST (Repetitive Element AneupLoidy Sequencing Fallopian Tube Aneuploidy in STIC) algorithm, and the remaining 36 STICs were included in the validation set (Supplementary Table S1). The procedures and collection of microdissected tissues were previously described (4). In addition, we included 12 HGSC specimens by manually dissecting tumor-enriched regions. Genomic DNA from individual specimens was extracted using the QIAmp FFPE DNA tissue kit (Qiagen, 56404).

### Immunohistochemistry (IHC)

The following antibodies were used for IHC: anti-p53 mouse mAb, anti–Ki-67 antibody, anti-mitochondrial cytochrome-c oxidase subunit 1 (MT-CO1) antibody, and anti-IGFBP2 antibody. Their sources and dilutions are listed in Supplementary Table S2. Antigen retrieval and IHC followed previous methods (28, 29). The staining patterns in HGSCs, STICs, and p53 signatures, MT-CO1 loss epithelium, as well as NFTE were recorded. We interpreted the p53-staining pattern as the missense mutation pattern when intense and diffuse nuclear immunoreactivity was detected in epithelial cells, null mutations when no staining signal was detectable, and wild-type pattern when weak and focal staining was recorded. The percentage of Ki-67–positive nuclei was determined among lesions from as many available cells and controls from at least 200 epithelial cells. Eight precursor lesions were known to harbor *TP53* mutations in this study: seven with missense mutations and one with a null mutation (3, 4). All the missense mutation lesions exhibited intense p53 staining, confirming the robustness of using immunoreactivity as a mutation surrogate. The formula H-score $= \Sigma$ (intensity score) $\times$ (% of lesion cells at a given intensity level) $\times$ 100 was used to semi-quantitatively evaluate immunoreactivity in epithelial cells. Intensity was scored as 0, 1, 2, or 3 by two pathologists (Y.-W. Chien and I.-M. Shih).

### Cell lines and colony formation assay

Two cell lines, including a human fallopian tube cell line, FT282 (established by the author, Ronny Drapkin, available in ATCC, CRL-3499, RRID:CVCL_A4AX; refs. 30, 31), and a high-grade serous ovarian cancer cell line, SKOV3 (ATCC, HTB-77, RRID:CVCL_0532), were used in this study. Both cell lines were obtained in 2015 and the authenticities were confirmed using short tandem repeat at the beginning of this study. The cells were cultured in RPMI-1640 (Gibco,

11875093) supplemented with 10% heat-inactivated FBS (Sigma, F4135), and 1% penicillin/streptomycin (Gibco 15140122). All cell lines were tested for *Mycoplasma* contamination using the universal mycoplasma detection kit (ATCC, 30–1012K) every two months during the study. The passage numbers for FT282 and SKOV3 from thawing were estimated to be 55 and 80, respectively. Lentiviruses containing 4 different shRNAs against MT-CO1 as well as vector control were obtained from OriGene. After treating the cells with lentivirus and polybrene (8 μg/mL) for 72 hours, cells were seeded at a density of 500 cells/well into 12-well plates. Cells from different groups were used for western blot analysis to determine knockdown efficiency. After 14–21 days, colonies were fixed with 100% ethanol, stained with 0.5% crystal violet, and quantified using ImageJ software (RRID: SCR_003070).

### Western blot analysis

Cell lysis buffer (Cell Signaling Technology, 9803S) supplemented with protease inhibitor (Roche) and PhosSTOP (Roche) was used for protein extraction. The protein was electrophoresed in 4%–15% polyacrylamide Mini-PROTEAN TGXTM Precast Protein Gels (Bio-Rad, 4561086), and then transferred to a polyvinylidene difluoride membrane (Bio-Rad). After blocking with 5% BSA in TBST for an hour at room temperature, the membrane was incubated with primary antibodies against MT-CO1 at 4°C overnight, followed by a 1-hour incubation with horseradish peroxidase–labeled secondary antibodies. The blot was then developed using ClarityTM Western ECL Blotting Substrate (Bio-Rad, 1705061). The antibodies used for blotting are listed in Supplementary Table S2.

### RealSeqS conditions

The method of RealSeqS has been detailed in a previous report (22). A single-primer pair (Forward: cgacgtaaaacgacggccagtNNNNNNNNNNNNNNNNNGGTGAAACCCCGTCTCTACA; Reverse: cacacaggaaacagctatgaccatgCCTCCTAAGTAGCTGGGACTACAG) was used to amplify approximately 350,000 genomic loci. PCR was performed in 25 μL reactions containing 7.25 μL of water, 0.125 μL of each primer with concentration of 100 μmol/L, 12.5 μL of NEBNext Ultra II Q5 Master Mix (New England Biolabs cat # M0544S), and 5 μL of DNA. We used a total of 2.5 ng of DNA for all samples. The cycling conditions were: one cycle of 98°C for 120 s, then 15 cycles of 98°C for 10 s, 57°C for 120 s, and 72°C for 120 s. Each sample was assessed in eight independent reactions, and the amount of DNA per reaction varied from 0.1 to 0.25 ng. A second round of PCR was then performed to add dual indexes (barcodes) to each PCR product before sequencing. The second round of PCR was performed in 25 μL reactions containing 7.25 μL of water, 0.125 μL of each primer, 12.5 μL of NEBNext Ultra II Q5 Master Mix (New England Biolabs cat # M0544S), and 5 μL of DNA containing 5% of the PCR product from the first round. The cycling conditions were: one cycle of 98°C for 120 s, then 15 cycles of 98°C for 10 s, 65°C for 15 s, and 72°C for 120 s. Amplified products from the second round were purified with AMPure XP beads (Beckman cat # a63880), as per the manufacturer's instructions, before sequencing and exclusion of fragment sizes <100 bps. As noted above, each sample was amplified in eight independent PCRs in the first round. Each of the eight independent PCRs was then re-amplified using index primers in the second PCR round. The sequencing reads from the 8 replicates were summed for the bioinformatic analysis but could also be assessed individually for quality control purposes.

All oligonucleotides were purchased from IDT, Inc. Sequencing was performed on an Illumina HiSeq 4000 using single end reads of 150 bps length. During the first round of PCR, degenerate bases at the 5′ end of one of the primers were used as molecular barcodes (unique identifiers, UID) to uniquely label each DNA template molecule. This ensured that each DNA template molecule was counted only once. In all instances in this study, the term "reads" refers to UID reads. Depending on the experiment, each read was sequenced on average 1.2 times. The average number of uniquely aligned reads was 8.7 million (interquartile range, 4.7–12.5 million). Any sample with fewer than one million reads was excluded (22, 23). Sequencing depth was the only quality control metric determining if a specific sample should be excluded.

The pipeline used to process the raw sequencing data is available at https://zenodo.org/record/3656943#.YaZZCdDMKUk. Briefly, the bioinformatic pipeline has a custom de-multiplexing step that requires exact matching of both indices. For each read, the pipeline removes the unique molecular barcode (the first 16 bases) and forward primer (the next 19 bases). The pipeline then searches for the reverse primer. Because we expected many amplicons to have non-perfect primer matching, we only searched for a small section of the reverse primer (AGTC, CCCA, TACT, or ACTT) during primer stripping. The remaining bases are aligned to the human reference genome assembly GRC37. An average of 51.1% of the total reads is uniquely aligned in this fashion. We are theoretically able to amplify up to 745,184 repetitive elements but typically only observe approximately 350,000 repetitive elements. A full list of the repetitive elements is included in our previous report (22). The bioinformatic pipeline generates a file with the observed counts at each locus. The following Python2 (RRID:SCR_008394) dependencies are required for the bioinformatics pipeline: argparse, json, logging, multiprocessing, and re. We used the following versions when processing the raw data: Python 2.7.14, argparse 1.1, json 2.0.9, logging (0.5.1.2), multiprocessing (0.70a1), and re (2.2.1).

### Detection of chromosome alterations and the REAL-FAST algorithm

Chromosomal alterations are identified when a sample's normalized read counts within a genomic region are significantly different from what would be expected in a euploid sample. Each sample is compared with a reference panel consisting of 30 euploid samples of genomic DNA from individuals without cancer. These samples were epithelium cells collected and purified from voided urine from young individuals (<25 years of age) and not included in the study. RealSeqS was performed on those 30 samples before the evaluation of experimental samples in our study. Each experimental sample was matched to a smaller subset ($n = 7$) of the larger reference panel ($n = 30$) that were most similar with respect to the amplicon distributions generated by RealSeqS based on a Euclidean distance. The statistical significance for the 39 non-acrocentric chromosome arms was then calculated using the equation below.

$$Z_{chr} = \frac{Observed_{chr} - \mu_{chr\ panel}}{\sigma_{chr\ panel}}$$

An arm was called aneuploid if $|Z_{chr}|>5$, gained if $Z_{chr} > 5$, and lost if $Z_{chr} < -5$. In addition to generating arm-level statistical significances, the circular binary algorithm (CBS) as distributed in the DNAcopy library (v1.58) within the R (v3.6.1) programming language was applied to 50-kb non-overlapping genomic intervals for each experimental sample (32). The CBS algorithm identifies sub-chromosomal focal alterations. A focal amplification for 19q12, 19q13.2, or 8q24 was called if CBS produced a sub-chromosomal segment surrounding the region of interest and had a $\log_2$ ratio >0.25. Next, on the basis of the

data obtained from the discovery set, we built the REAL-FAST algorithm to molecularly classify STIC, p53 signature, and NFTE into different clusters or paths.

### Statistical analysis

The data were shown as the mean with one standard error. Unless otherwise noted, the statistical significance of the difference between two groups was assessed using an unpaired, two-tailed Student *t* test or Fisher's exact test. Differences were considered significant for the *P* value of <0.05. Figures were prepared using the Prism software.

### Data availability

The data generated in this study can be requested upon approval (European Genome-Phenome Archive, EGAD50000000013).

## Results

### Normal-appearing FTE harbors low-level aneuploidy

We performed RealSeqS on a total of 150 DNA samples, including 138 samples from fallopian tubes and 12 HGSCs. **Figure 1A** depicted the flow of the study design. H&E-stained and p53-immunostained slides were used to guide the LCM (**Fig. 1B**). **Table 1** summarizes age, race, pathologic finding, status of germline mutation, concurrent cancer, and clinical follow-up in all patients. Supplementary Table S1 lists the numbers of cases and patients. In this study, we use the term, histologically unremarkable FTE (HU-FTE), to indicate normal-appearing epithelium from fallopian tubes. HU-FTE included randomly selected HU-FTE (called "NFTE"), "p53 signature" defined by intense nuclear p53 antibody immunoreactivity, a pattern indicative of missense *TP53* mutations (33), and the "MT-CO1 protein loss region" defined by complete absence or greatly reduced MT-CO1 immunoreactivity in a discrete epithelial stretch (Supplementary Fig. S1A). The epithelial cells in both p53 signature and *MT-CO1* protein loss regions were morphologically indistinguishable to adjacent NFTE on the basis of H&E staining.

*TP53* mutations have long served as a molecular genetic marker for analyzing clonal relationships in cancer research (8, 27, 34, 35). *MT-CO1* is a mitochondrial DNA encoding cytochrome C oxidase-1 that is constitutively expressed in all normal cells. Loss of its expression due to inactivating heteroplasmic mutations in mitochondria has also been used as a convenient marker for lineage tracing in normal tissue (24–27). All the NFTE samples showed either an absence or a low level of aneuploidy (**Fig. 1C**). Although they were histologically unremarkable, the epithelium in all 26 (100%) p53 signatures showed deletion involving entire chr17 (22 cases) or chr17 p/q-arm (three cases) that was not detected in either NFTE or in any of 20 *MT-CO1* loss regions ($P < 0.01$; **Table 2**).

Among all MT-CO1 loss regions, one showed a focal break in 500 kb region in chr17p. p53 IHC was performed on the original slide that was stained with *MT-CO1* antibody, which confirmed that this stretch was not a p53 signature (Supplementary Fig. S1B). Because deficiency in DNA damage repair has been reported as a mechanism contributing to chromosome instability (36–38), we also compared the degree of aneuploidy between *MT-CO1* loss epithelial stretches derived from women with and without germline *BRCA1/2* mutation(s). The results showed that *BRCA* germline mutations were not associated with higher aneuploidy at arm level in NFTE (data not shown).

*MT-CO1* mutations were reported as potentially neutral passenger mutations, appearing not to confer known positive or negative proliferative fitness in normal cells (39). To validate this finding in the context of this study, we performed *MT-CO1* gene knockdown using lentivirus carrying shRNAs targeting *MT-CO1* on the FT282 fallopian tube epithelial cell line and on the SKOV3 ovarian cancer cell line. In both FT282 and SKOV3 cell lines, *MT-CO1* knockdown did not affect colony formation ability compared with vector control (Supplementary Fig. S1C and S1D). Western blot analysis confirmed the knockdown efficiency (Supplementary Fig. S1E).

### STICs are characterized by pronounced and non-random aneuploidy patterns

We used the criteria previously reported for morphological classification of STICs. In short, STIC cells lack cilia and have a various degree of nuclear enlargement, hyperchromasia, increased nuclear-to-cytoplasmic ratios, loss of polarity, prominent nucleoli, apoptotic bodies, and mitotic figures (6, 7). On the basis of analyzing aneuploidy in 73 STICs, we observed that STICs had a significantly higher incidence of chromosomal arm gain or loss than HU-FTE, including p53 signatures and MT-CO1 loss regions. After classifying STICs into proliferatively active and proliferatively dormant groups, we found proliferatively active STICs had a higher aneuploidy level than dormant STICs ($P < 0.05$; **Fig. 1C**) whereas dormant STICs exhibited higher amount of gain or loss of chromosomal arms than p53 signatures ($P = 0.04$) and NFTE ($P < 0.01$). We also analyzed 12 HGSC samples and found their aneuploidy level indistinguishable from active STICs ($P = 0.71$; **Fig. 1C**; Supplementary Fig. S2).

We next sought to identify chromosome changes most likely accompanying the tumor progression. We selected the most commonly occurring DNA copy-number changes in each lesion subtype. We found that chr17 deletion (whole p/q arm or focal) was a universal event in all 98 lesions, including STIC and p53 signatures studied (Supplementary Table S3). Thus, chr17 harboring *TP53* appears to be the first chromosome where DNA copy-number changes occur in HGSC initiation.

**Table 2** lists the chromosomal regions showing DNA copy-number gain or loss in STICs. As compared with p53 signatures, we observed that 16 (84.20%) of 19 proliferatively dormant STICs contained additional chromosomal abnormalities, mainly chr22q loss. We also found that 46 (85.2%) of 54 proliferatively active STICs, as compared with dormant STICs, harbored specific gains in chr19q harboring the driver gene *CCNE1*, or in chr8q arm harboring the driver genes, including *MYC* and *RECQL4*; **Fig. 1D–H**; **Table 2**). A notable finding from the RealSeqS data was that amplification in *CCNE1* and *MYC/RECQL4* appeared to be mutually exclusive ($P < 0.01$). Overall, of the 54 active STICs, 17 harbored 19q12 amplification only, 10 harbored 8q24 amplification only, and only 4 showed alterations in both regions (Supplementary Table S4).

Next, we assessed whether the regions showing DNA copy-number gain or loss in STICs were also present in HGSC (40). **Table 2** lists those common regions that contain several known cancer-driver genes. On the basis of the total number of break points in all chromosomes, we detected significantly more break points in proliferatively active STICs and HGSCs than in dormant STICs, p53 signatures, and normal control fallopian tube samples (**Fig. 1I**). Taken together, the results suggest that progression from HGSC precursor lesions to overt HGSC is associated with a non-random increase in chromosomal abnormalities.

### An aneuploidy-based molecular classification identifies different precursor lesions

Pathology diagnosis of STICs can be challenging because of the subjective nature of recognizing these lesions despite the morphological criteria that has been proposed (6). It is not surprising that even when adjunct immunostaining is applied, the reproducibility of STIC

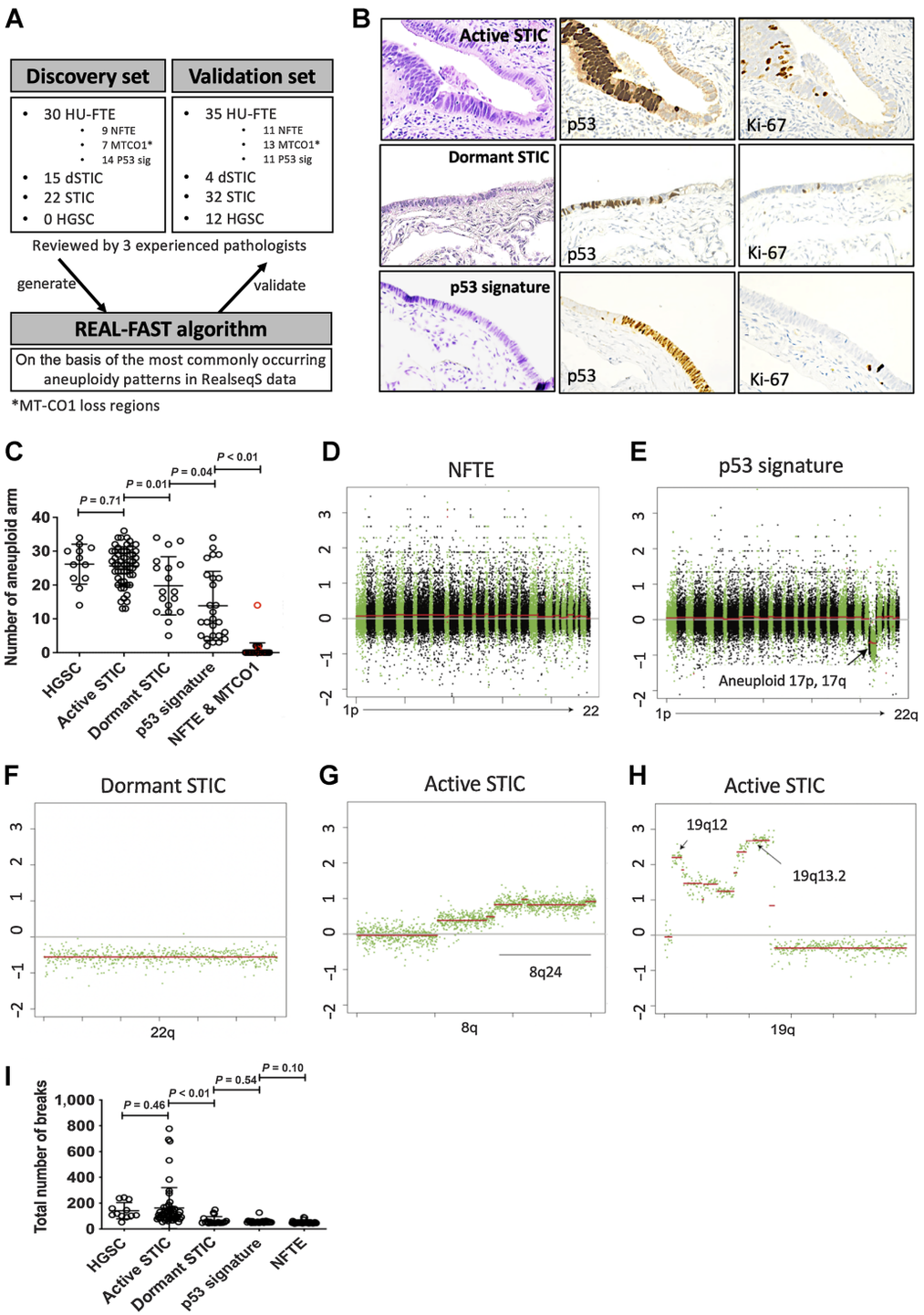


**Figure 1.**

Representative H&E (hematoxylin and eosin) and IHC and aneuploidy profile of the lesions studied. **A,** Flow chart of the study design. **B,** Representative images of H&E, p53, and Ki-67 IHC of proliferatively active STIC (top), proliferatively dormant STIC (middle), and p53 signature (bottom). **C,** Scatter plot of the number of aneuploid arms in different lesions. Red circles represent the 20 MT-CO1 loss regions analyzed in the study. **D,** Representative image of RealSeqS data of randomly selected histologically unremarkable fallopian tube epithelium (NFTE) derived from one patient. Each dot represents one repetitive element sequenced. The *y*-axis indicates $\log_2$ value of ratio between observed and expected counts. Mean relative copy-number changes at different loci are shown as red lines. **E,** Representative RealSeqS data of a p53 signature. The arrow indicates loss of both chr17 p-arm and q-arm. **F,** Representative RealSeqS data showing additional chr22q loss in dormant STIC compared with p53 signature. **G** and **H,** Representative RealSeqS data showing additional chr8q24, chr19q12, and chr19q13.2 gain in active STIC compared with dormant STIC. **I,** Scatter plot showing total number of chromosomal break points across different sample types analyzed. Note: **C** and **I** were prepared using the Prism software.

**Table 1.** Clinical information, p53 staining pattern, Ki-67 proliferation index, and pathology diagnosis of all lesions studied.

| Case number | FTE# | Age | Pathology diagnosis | Molecular diagnosis | Path | TP53 pattern | Ki67 index | Germline mutations | Concurrent HGSOC | Tumor staging (FIGO) | Subsequent HGSOC during follow-up (progression-free survival, months) | Follow-up duration (months) |
|---|---|---|---|---|---|---|---|---|---|---|---|---|
| 1 | FTE-24 | 73 | dSTIC | dSTIC | Path-4 | Missense | 1.2 | NA | No | None | No | 53 |
| | FTE-17 | | STIC | dSTIC | Path-4 | Missense | 1 | | | | | |
| | FTE-40 | | dSTIC | dSTIC | Path-4 | Missense | 2 | | | | | |
| | FTE-41 | | dSTIC | dSTIC | Path-4 | Missense | 1 | | | | | |
| | FTE-18 | | p53 sig | p53 sig | Path-5 | Missense | 2 | | | | | |
| 2 | FTE-13 | 72 | MT-CO1 loss region | NFTE | Path-1 | NA | NA | NA | No | None | No | 77 |
| | FTE-15 | | MT-CO1 loss region | NFTE | Path-1 | NA | NA | | | | | |
| 3 | FTE-46 | 51 | dSTIC | p53 sig | Path-5 | Missense | 2 | NA | No | None | No | 36 |
| | FTE-108 | | STIC | dSTIC | Path-4 | Nonsense | 55 | | | | | |
| 4 | FTE-119 | 68 | STIC | STIC | Path-2 | NA | 32 | NA | Yes | IIIC | No | 22 |
| 5 | FTE-115 | 60 | STIC | STIC | Path-3 | Missense | 11 | BRCA1 (pathogenic) | No | IA | No | 65 |
| 6 | FTE-126 | 59 | STIC | STIC | Path-2 | NA | 69 | VUS BRCA2 and MLH1 | Yes | IIIC | No | 5 (deceased) |
| | FTE-127 | | STIC | STIC | Path 2 | NA | 41 | | | | | |
| | FTE-138 | | HGSC | STIC | Path-2 | NA | NA | | | | | |
| 7 | FTE-128 | 34 | STIC | STIC | Path-3 | NA | 41 | BRCA1 (pathogenic) | Yes | IA | No | 40 |
| | FTE-139 | | HGSC | STIC | Path-2 | NA | 35 | | | | | |
| 8 | FTE-51 | 68 | dSTIC | STIC | Path-2 | Missense | 1 | NA | No | None | No | 123 |
| 9 | FTE-104 | 40 | STIC | p53 sig | Path-5 | Missense | NA | NA | No | IA | No | 27 |
| 10 | FTE-129 | 68 | STIC | STIC | Path-2 | NA | 39 | RAD51C (pathogenic) | Yes | IIA | No | 39 |
| | FTE-130 | | STIC | STIC | Path-2 | NA | 43 | | | | | |
| | FTE-131 | | STIC | STIC | Path-2 | NA | 37 | | | | | |
| | FTE-132 | | STIC | STIC | Path-3 | NA | 33 | | | | | |
| 11 | FTE-14 | 71 | MT-CO1 loss region | NFTE | Path-1 | NA | NA | NA | No | None | No | 39 |
| | FTE-16 | | MT-CO1 loss region | NFTE | Path-1 | NA | NA | | | | | |
| | FTE-12 | | MT-CO1 loss region | NFTE | Path-1 | NA | NA | | | | | |
| 12 | FTE-26 | 58 | p53 sig | dSTIC | Path-4 | NA | 5.3 | Lynch syndrome | No | None | No | 37 |
| | FTE-44 | | dSTIC | dSTIC | Path-4 | NA | 2 | | | | | |
| | FTE-45 | | dSTIC | dSTIC | Path-4 | NA | 6 | | | | | |
| 13 | FTE-71 | 44 | STIC | STIC | Path-3 | Missense | 25 | VUS, ATM and RAD50 | No | IA | No | 98 |
| | FTE-50 | | dSTIC | STIC | Path-3 | Missense | 5.2 | | | | | |
| 14 | FTE-22 | 72 | dSTIC | dSTIC | Path-4 | Missense | 4.3 | NA | Yes | IIIC | NA | 44 |
| | FTE-48 | | dSTIC | STIC | Path-3 | Missense | 1 | | | | | |
| | FTE-101 | | STIC | STIC | Path-3 | Missense | 53 | | | | | |
| | FTE-110 | | STIC | STIC | Path-2 | Missense | 51 | | | | | |
| | FTE-144 | | HGSC | STIC | Path-3 | Missense | 41 | | | | | |
| 15 | FTE-43 | 72 | dSTIC | dSTIC | Path-4 | Missense | 2 | NA | No | None | No | 37 |
| 16 | FTE-59 | 85 | STIC | STIC | Path-2 | Null | 78 | NA | Yes | IIIB | No | 3 (loss of follow-up) |
| | FTE-58 | | STIC | STIC | Path-2 | Null | 70 | | | | | |
| | FTE-142 | | HGSC | STIC | Path-2 | Null | 72 | | | | | |
| 17 | FTE-65 | 62 | STIC | STIC | Path-2 | Missense | 40 | BRCA1 (pathogenic) | Yes | IIIA2 | No | 44 |
| | FTE-141 | | HGSC | STIC | Path-3 | Missense | NA | | | | | |

*(Continued on the following page)*

**Table 1.** Clinical information, p53 staining pattern, Ki-67 proliferation index, and pathology diagnosis of all lesions studied. (Cont'd)

| Case number | FTE# | Age | Pathology diagnosis | Molecular diagnosis | Path | TP53 pattern | Ki67 index | Germline mutations | Concurrent HGSOC | Tumor staging (FIGO) | Subsequent HGSOC during follow-up (progression-free survival, months) | Follow-up duration (months) |
|---|---|---|---|---|---|---|---|---|---|---|---|---|
| 18 | FTE-10 | 71 | MT-CO1 loss region | NFTE | Path-1 | NA | NA | NA | Yes | None | No | 108 |
| | FTE-11 | | MT-CO1 loss region | NFTE | Path-1 | NA | NA | | | | | |
| 19 | FTE-55 | 41 | STIC | dSTIC | Path-4 | Missense | 81 | BRCA2 (pathogenic) | No | None | No | 37 |
| | FTE-08 | | NFTE | NFTE | Path-1 | NA | 2 | | | | | |
| | FTE-09 | | NFTE | NFTE | Path-1 | NA | 2 | | | | | |
| 20 | FTE-78 | 32 | NFTE | NFTE | Path-1 | NA | 3 | NA | Yes | IIIC | No | 24 |
| | FTE-116 | | STIC | STIC | Path-3 | NA | 13 | | | | | |
| | FTE-134 | | HGSC | STIC | Path-3 | NA | 23 | | | | | |
| 21 | FTE-79 | 65 | NFTE | NFTE | Path-1 | NA | 1 | NA | Yes | IIIC | No | 36 |
| | FTE-117 | | STIC | STIC | Path-3 | NA | 21 | | | | | |
| | FTE-118 | | STIC | STIC | Path-2 | NA | 19 | | | | | |
| | FTE-135 | | HGSC | STIC | Path-3 | NA | 24 | | | | | |
| 22 | FTE-76 | 76 | NFTE | NFTE | Path-1 | NA | 4 | NA | No | None | No | 35 |
| | FTE-77 | | NFTE | NFTE | Path-1 | NA | 2 | | | | | |
| 23 | FTE-67 | 46 | STIC | STIC | Path-3 | Nonsense | 62 | BRCA1 (pathogenic) | No | IA | No | 36 |
| | FTE-66 | | STIC | STIC | Path-3 | Nonsense | 78 | | | | | |
| 24 | FTE-23 | 60 | dSTIC | dSTIC | Path-4 | Missense | NA | NA | No | None | No | 51 |
| 25 | FTE-28 | 70 | p53 sig | p53 sig | Path-5 | Missense | 1.4 | NA | Yes | IVB | Yes (3) | 36 |
| | FTE-03 | | NFTE | NFTE | Path-1 | NA | 1.5 | | | | | |
| 26 | FTE-64 | 67 | STIC | STIC | Path-3 | Missense | 25 | NA | Yes | I | Yes (31) | 44 |
| 27 | FTE-04 | 74 | NFTE | NFTE | Path-1 | NA | 2 | NA | No | None | No | 50 |
| 28 | FTE-25 | 52 | p53 sig | dSTIC | Path-4 | Missense | 2.9 | NA | No | None | No | 63 |
| 29 | FTE-56 | 69 | STIC | STIC | Path-2 | Missense | 30 | NA | Yes | IIB | Yes (20) | 62 |
| 30 | FTE-57 | 50 | STIC | STIC | Path-2 | Null | 38 | NA | No | None | No | 16 (deceased due to MMMT) |
| | FTE-02 | | NFTE | NFTE | Path-1 | NA | 5 | | | | | |
| 31 | FTE-49 | 55 | dSTIC | STIC | Path-3 | Missense | 1 | BRCA1 (pathogenic) | No | None | No | 56 |
| 32 | FTE-37 | 67 | p53 sig | p53 sig | Path-5 | Missense | NA | NA | No | None | No | 30 |
| | FTE-62 | | STIC | STIC | Path-3 | Missense | 30 | | | | | |
| | FTE-29 | | p53 sig | p53 sig | Path-5 | Missense | NA | | | | | |
| | FTE-36 | | p53 sig | STIC | Path-3 | Missense | NA | | | | | |
| | FTE-30 | | p53 sig | p53 sig | Path-5 | Missense | NA | | | | | |
| | FTE-32 | | p53 sig | p53 sig | Path-5 | Missense | NA | | | | | |
| | FTE-35 | | p53 sig | p53 sig | Path-5 | Missense | NA | | | | | |
| | FTE-34 | | p53 sig | p53 sig | Path-5 | Missense | NA | | | | | |
| | FTE-31 | | p53 sig | p53 sig | Path-5 | Missense | NA | | | | | |
| | FTE-33 | | p53 sig | p53 sig | Path-5 | Missense | NA | | | | | |
| | FTE-19 | | p53 sig | p53 sig | Path-5 | Missense | NA | | | | | |
| 33 | FTE-120 | 48 | STIC | STIC | Path-3 | NA | 23 | BRCA1 (pathogenic) | Yes | IIIC | No | 21 |
| | FTE-136 | | HGSC | STIC | Path-2 | NA | 65 | | | | | |
| 34 | FTE-72 | 44 | NFTE | NFTE | Path-1 | NA | 2 | BRCA2 (pathogenic) | No | IA | No | 31 |
| | FTE-109 | | STIC | STIC | Path 3 | Missense | 62 | | | | | |
| 35 | FTE-100 | 71 | dSTIC | dSTIC | Path-4 | Missense | 16 | NA | Yes | IVA | Yes (12) | 22 |

*(Continued on the following page)*

**Table 1.** Clinical information, p53 staining pattern, Ki-67 proliferation index, and pathology diagnosis of all lesions studied. (Cont'd)

| Case number | FTE# | Age | Pathology diagnosis | Molecular diagnosis | Path | TP53 pattern | Ki67 index | Germline mutations | Concurrent HGSOC | Tumor staging (FIGO) | Subsequent HGSOC during follow-up (progression-free survival, months) | Follow-up duration (months) |
|---|---|---|---|---|---|---|---|---|---|---|---|---|
| | FTE-114 | | STIC | STIC | Path-3 | Missense | 6 | | | | | |
| 36 | FTE-73 | 83 | NFTE | NFTE | Path-1 | NA | 4 | NA | No | None | No | 22 |
| | FTE-74 | | NFTE | NFTE | Path-1 | NA | 1 | | | | | |
| | FTE-75 | | NFTE | NFTE | Path-1 | NA | 2 | | | | | |
| 37 | FTE-60 | 65 | STIC | STIC | Path-2 | Nonsense | 5 | VUS in AIP and HOXB13 | No | None | No | 54 |
| | FTE-61 | | STIC | STIC | Path-2 | Nonsense | NA | | | | | |
| | FTE-52 | | STIC | dSTIC | Path-4 | Nonsense | 21 | | | | | |
| 38 | FTE-112 | 71 | STIC | STIC | Path-2 | Missense | 63 | NA | No | None | No | NA (loss of follow-up) |
| | FTE-113 | | STIC | STIC | Path-2 | Missense | 65 | | | | | |
| 39 | FTE-140 | 67 | HGSC | STIC | Path-2 | Missense | NA | NA | Yes | IVB | Yes (24) | 42 |
| 40 | FTE-63 | 75 | STIC | STIC | Path-3 | Missense | 31 | NA | Yes | NA | NA | NA (consult case) |
| 41 | FTE-06 | 56 | NFTE | NFTE | Path-1 | NA | 1 | NA | No | None | No | 119 |
| | FTE-98 | | dSTIC | dSTIC | Path-4 | Missense | 2 | | | | | |
| | FTE-99 | | dSTIC | dSTIC | Path-4 | Missense | 2 | | | | | |
| | FTE-97 | | p53 sig | p53 sig | Path-5 | Missense | 3 | | | | | |
| 42 | FTE-47 | 66 | dSTIC | STIC | Path-3 | Missense | 2 | NA | No | None | No | 39 |
| 43 | FTE-107 | 67 | STIC | STIC | Path-2 | Missense | 13 | NA | Yes | IIIC | Yes (2) | 39 (loss of follow-up) |
| | FTE-145 | | HGSC | STIC | Path-2 | Missense | NA | | | | | |
| 44 | FTE-69 | 66 | STIC | STIC | Path-2 | Missense | 70 | BRCA2 (pathogenic) | No | None | No | |
| 45 | FTE-70 | 41 | STIC | STIC | Path-3 | Missense | 20 | BRCA2 (pathogenic) | Yes | IIIC | Yes (20) | 86 |
| | FTE-53 | | STIC | STIC | Path-3 | Missense | 10 | | | | | |
| 46 | FTE-106 | 69 | STIC | STIC | Path-2 | Missense | 81 | NA | Yes | NA | NA | NA |
| | FTE-143 | | HGSC | STIC | Path-2 | Missense | NA | | | | | |
| 47 | FTE-102 | 58 | STIC | STIC | Path-2 | Missense | 56 | NA | Yes | NA | NA | NA |
| | FTE-103 | | STIC | STIC | Path-2 | Missense | 52 | | | | | |
| | FTE-105 | | STIC | STIC | Path-2 | Missense | 60 | | | | | |
| | FTE-111 | | STIC | STIC | Path-2 | Missense | 82 | | | | | |
| 48 | FTE-121 | 46 | STIC | STIC | Path-2 | NA | 42 | NA | Yes | IIIA1 | No | 30 |
| 49 | FTE-122 | 57 | STIC | STIC | Path-3 | NA | 41 | NA | Yes | IA | No | 5 days (loss of follow-up) |
| | FTE-123 | | STIC | STIC | Path-3 | NA | 45 | | | | | |
| | FTE-124 | | STIC | STIC | Path-3 | NA | 38 | | | | | |
| | FTE-80 | | NFTE | NFTE | Path-1 | NA | 3 | | | | | |
| 50 | FTE-125 | 84 | HGSC | STIC | Path-3 | NA | 61 | NA | Yes | IIIB | No | 12 |
| | FTE-81 | | NFTE | NFTE | Path-1 | NA | 2 | | | | | |
| 51 | FTE-42 | NA | dSTIC | dSTIC | Path-4 | NA | 1 | NA | NA | NA | NA | NA |
| 52 | FTE-01 | 59 | NFTE | NFTE | Path-1 | NA | 4 | NA | No | None | No | 1 (loss of follow-up) |
| | FTE-54 | | STIC | dSTIC | Path-4 | Missense | 25 | | | | | |

*(Continued on the following page)*

**Table 1.** Clinical information, p53 staining pattern, Ki-67 proliferation index, and pathology diagnosis of all lesions studied. (Cont'd)

| Case number | FTE# | Age | Pathology diagnosis | Molecular diagnosis | Path | TP53 pattern | Ki67 index | Germline mutations | Concurrent HGSOC | Tumor staging (FIGO) | Subsequent HGSOC during follow-up (progression-free survival, months) | Follow-up duration (months) |
|---|---|---|---|---|---|---|---|---|---|---|---|---|
| 53 | FTE-07 | 49 | NFTE | NFTE | Path-1 | NA | 1 | BRCA2 (pathogenic) | No | None | No | 1 (loss of follow-up) |
| | FTE-68 | | STIC | STIC | Path-2 | Missense | 10 | | | | | |
| 54 | FTE-05 | 70 | NFTE | NFTE | Path-1 | NA | 3 | NA | No | None | No | 106 |
| | FTE-20 | | STIC | STIC | Path-2 | Missense | 1 | | | | | |
| 55 | FTE-84 | 58 | MT-CO1 loss region | NFTE | Path-1 | NA | NA | BRCA1 (pathogenic) | No | None | No | 73 |
| | FTE-85 | | MT-CO1 loss region | NFTE | Path-1 | NA | NA | | | | | |
| | FTE-86 | | MT-CO1 loss region | NFTE | Path-1 | NA | NA | | | | | |
| | FTE-87 | | MT-CO1 loss region | NFTE | Path-1 | NA | NA | | | | | |
| 56 | FTE-88 | 59 | MT-CO1 loss region | NFTE | Path-1 | NA | NA | BRCA2 (pathogenic) | No | None | No | 75 |
| | FTE-89 | | MT-CO1 loss region | NFTE | Path-1 | NA | NA | | | | | |
| | FTE-91 | | MT-CO1 loss region | NFTE | Path-1 | NA | NA | | | | | |
| | FTE-92 | | MT-CO1 loss region | NFTE | Path-1 | NA | NA | | | | | |
| 57 | FTE-90 | 69 | MT-CO1 loss region | NFTE | Path-1 | NA | NA | BRCA2 (pathogenic) | No | None | No | 48 |
| | FTE-93 | | MT-CO1 loss region | NFTE | Path-1 | NA | NA | | | | | |
| | FTE-94 | | MT-CO1 loss region | NFTE | Path-1 | NA | NA | | | | | |
| 58 | FTE-82 | 60 | MT-CO1 loss region | NFTE | Path-1 | NA | NA | NA | No | None | No | 41 |
| | FTE-83 | | MT-CO1 loss region | p53 sig | Path-5 | NA | NA | | | | | |
| 59 | FTE-95 | 53 | NFTE | NFTE | Path-1 | NA | 4 | NA | No | None | No | 15 |
| | FTE-133 | | STIC | STIC | Path-3 | Missense | 41 | | | | | |
| 60 | FTE-146 | 54 | p53 sig | NFTE | Path-1 | Missense | NA | VUS in TP53 | No | None | No | 8 |
| | FTE-147 | 54 | p53 sig | p53 sig | Path-5 | Missense | NA | | | | | |
| | FTE-148 | 54 | p53 sig | p53 sig | Path-5 | Missense | NA | | | | | |
| | FTE-149 | 54 | p53 sig | p53 sig | Path-5 | Missense | NA | | | | | |
| | FTE-150 | 54 | p53 sig | p53 sig | Path-5 | Missense | NA | | | | | |
| | FTE-151 | 54 | p53 sig | p53 sig | Path-5 | Missense | NA | | | | | |
| | FTE-152 | 54 | p53 sig | p53 sig | Path-5 | Missense | NA | | | | | |
| | FTE-153 | 54 | p53 sig | p53 sig | Path-5 | Missense | NA | | | | | |
| | FTE-154 | 54 | p53 sig | p53 sig | Path-5 | Missense | NA | | | | | |
| | FTE-155 | 54 | p53 sig | p53 sig | Path-5 | Missense | NA | | | | | |
| 61 | FTE-156 | 57 | p53 sig | dSTIC | Path-4 | Missense | 0 | BRCA1 (pathogenic) | No | None | No | NA |
| | FTE-157 | 57 | dSTIC | p53 sig | Path-5 | Missense | 3 | | | | | |

Abbreviations: dSTIC, dormant STIC; HGSOC, high-grade serous ovarian cancer; NA, not available; p53 sig, p53 signature; STIC, serous tubal intraepithelial carcinoma; VUS, variant of unknown significance.

**Table 2.** Prevalence of commonly HGSC-associated altered chromosomal regions in the precursor lesions.

| Involved genomic loci | Gene | Gain/loss | NFTE | MT-CO1 loss region | p53 signature | Dormant STIC | Active STIC | HGSC |
|---|---|---|---|---|---|---|---|---|
| **15q21.1** | *CDH1* | Loss | 0% | 0% | 28% | 11% | 52% | 25% |
| **16q24.3** | *FANCA* | Loss | 0% | 0% | 0% | 5% | 48% | 58% |
| **9p21.3** | *CDKN2A* | Loss | 10% | 0% | 8% | 37% | 52% | 67% |
| **17 whole chromosome** | *TP53, BRCA1, NF1* | Loss | 0% | 0% | 88% | 95% | 65% | 50% |
| (17p full-arm only) | *TP53* | Loss | 0% | 0% | 8% | 0% | 20% | 25% |
| (17q full-arm only) | *BRCA1, NF1* | Loss | 0% | 0% | 4% | 0% | 7% | 0% |
| **22q arm** | | Loss | 0% | 0% | 8% | 84% | 78% | 83% |
| **19q12** | *CCNE1* | Gain | 0% | 0% | 0% | 5% | 39% | 42% |
| **19q.13.2** | | Gain | 0% | 0% | 0% | 5% | 28% | 33% |
| **8q24** | *MYC, RECQL4* | Gain | 5% | 0% | 0% | 0% | 26% | 50% |
| **8q arm** | | Gain | 0% | 0% | 4% | 26% | 48% | 42% |
| **3q26.2** | *MECOM* | Gain | 0% | 0% | 8% | 0% | 44% | 75% |
| **11q13.5** | *RSF-1* | Gain | 0% | 0% | 0% | 0% | 22% | 25% |
| **19p13.2** | *NACC1* | Gain | 0% | 0% | 4% | 16% | 41% | 58% |

lesions is, at best, only modest (41, 42). Therefore, we intended to establish an algorithm to distinguish among STIC lesions on the basis of aneuploidy patterns, and to identify molecular subgroups of STICs with unique biological features. Among the 73 STICs studied, we selected the first 37 (in an order of acquisition) as a training set and the remaining 36 as a validation set (**Fig. 1A**; Supplementary Table S1). We generated an algorithm called "REAL-FAST" (RealSeqS-based algorithm for fallopian tube aneuploidy pattern in STIC). REAL-FAST applies a binary decision tree (yes or no) that separates samples into two categories according to their unique aneuploidy patterns. In each category, the algorithm uses another decision tree to further separate cases according to their aneuploidy pattern, and so on. REAL-FAST provides an unsupervised classification system agnostic of pathology diagnoses.

REAL-FAST identified five distinct "Paths" (or groups), from Path 1 to Path 5. We have outlined the different Paths and their major characteristic chromosomal changes in **Fig. 2A**. First, we correlated different Paths with their pathology features and proliferative activity. Our results showed that Path-2, Path-3, and Path-4 corresponded to histologically diagnosed STICs, Path-5 to p53 signatures, and Path-1 to NFTE and MT-CO1 loss regions. The majority of proliferatively active STICs belonged to Path-2 and Path-3, whereas the dormant STICs to Path-4 (**Fig. 2A**). Among different Paths, the highest Ki-67–labeling index was detected in Path-2 followed by Path-3 and Path-4, whereas Ki-67–labeling index in Path-5 and Path-1 was similar to the background level in HU-FTE (**Fig. 2B**). We also performed immunostaining against IGFBP2, a marker known to be expressed in proliferative STICs (29), on lesions belonging to different Paths. The results showed Path-2 has the significantly higher IGFBP2 expression level compared with Path-3 and Path-4 ($P < 0.01$; **Fig. 2C**).

Alongside proliferative activity, we found that 22 (88%) of 25 Path-2 STICs were characterized by discohesive growth of STICs, in which individual or small clusters of STIC cells were loosely attached or detached from the lesion surface (**Fig. 2D**). In contrast, none of Path-4 STICs showed similar morphological features. STICs from Path-2 alone or from Path-2/Path-3 were more frequently to show discohesive growth than were Path-4 STICs ($P < 0.01$). Differences between Path-2 and Path-3/Path-4 and between Path-3 and Path-4 were significant as well. However, there were no significant differences between Path-2 and Path-3 STICs (Supplementary Table S5). **Figure 2E** summarized major aneuploidy patterns in different precancer lesions in fallopian tubes. In this training set, the concordance between the molecular and pathologic classification of STICs (both active and dormant) was 95.5% (63 out of 67 regions; **Table 3**).

### Performance of REAL-FAST in an independent cohort

To determine the performance of REAL-FAST, we analyzed the second (validation) cohort that was independent and non-overlapping with those in the training set. The validation cohort included 71 regions of FTE: 25 HU-FTE (including p53 signature, MT-CO1 loss regions, and NFTE), 36 STICs, and 12 HGSCs from 33 women with or without concurrent HGSC (**Fig. 1A**; Supplementary Table S1). Overall, the sensitivity and specificity of REAL-FAST in predicting histologically defined STICs and HGSCs were 95.8% and 97.14%, respectively. Both molecular and corresponding pathology diagnoses of individual samples were presented in **Table 4**. Moreover, all 12 HGSCs were molecular classified as either Path-2 (7 cases) or Path-3 (5 cases). On the basis of the REAL-FAST analysis, we did not discern any unique aneuploidy pattern between all STICs and HGSC, and between incidental active STIC and HGSC. We also compared the distribution of incidental active STIC with the lesions associated with HGSC according to different aneuploidy groups. Because Path-2 and Path-3 lesions had copy-number gains in two HGSC-related genes, *CCNE1* and *MYC*, respectively, we combined them then compared with the rest of the Paths (Path-1, -4, -5). We found that lesions with HGSC were more frequent in Path-2/Path-3 than the incidental cases ($P = 0.017$). There was no statistical significance by comparing incidental lesions and lesions with HGSC using other groupings (**Figs. 1C** and **2**; Supplementary Fig. S2 and Supplementary Table S6). For the discrepant cases, only one (FTE-156) out of the 35 HU-FTE were classified as Path-4, the dormant STIC group. Two pathology-diagnosed STICs among 36 STICs, FTE-157 and FTE-104, were molecularly classified as a p53 signature. Representative histology images of the lesions with discrepant pathology diagnosis and molecular classification are shown in Supplementary Fig. S3. The RealSeqS data for each lesion subtype at each decision point are summarized in Supplementary Table S3.

## Discussion

Intercepting ovarian cancer by surgical removal of fallopian tubes prophylactically has offered the current best approach to prevent

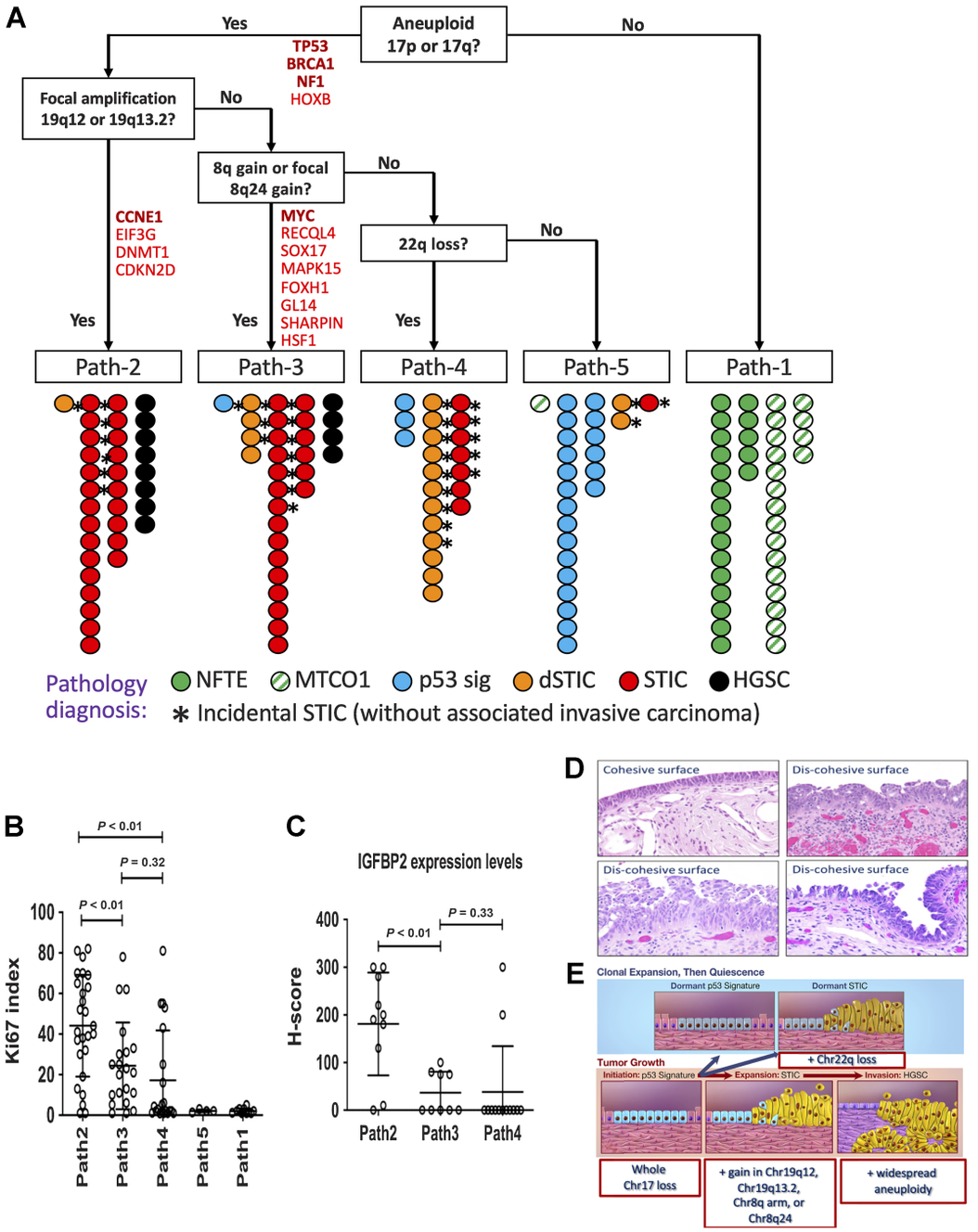


**Figure 2.**

Aneuploidy-based algorithm for the diagnosis of NFTE, precursor lesions, and HGSC. **A,** REAL-FAST algorithm classifies various types of FTE into five different Paths or groups on a basis of aneuploidy found in different chromosomal arms. The individual specimens (filled circles) are colored according to their pathology diagnoses. The cancer-associated genes with copy-number changes at each decision point are indicated and bolds represent the most relevant genes to HGSC. *, incidental STIC; dSTIC, proliferatively dormant STIC. **B,** The proliferative activity (Ki-67–labeling index) among different molecular groups. **C,** IGFBP2 expression levels among different molecular groups. **D,** Representative photomicrographs (H&E) from four different STICs showing either discohesive or cohesive growth. **E,** Schematic summary of major aneuploidy patterns in different precancer lesions in fallopian tubes. Figure adopted from Shih and colleagues (2). Illustration by Lydia Gregg 2021 JHU AMM. Note: **B** and **C** were prepared using the Prism software.

ovarian cancer, especially in women with genetic predisposition in developing the disease. There are at least two major questions facing those high-risk women after their fallopian tubes are surgically excised. First, a notable number of those salpingectomy specimens contain incidental HGSCs and STICs that challenge the clinical decision if those apparently ovarian cancer–free women need chemotherapy, close imaging-based surveillance, and/or staging biopsy. Second, pathology diagnosis of STICs can be difficult and non-reproducible

**Table 3.** Correlations between molecular prediction and pathology diagnosis in the discovery set.

| **Specimen** | **FTE-1** | **FTE-2** | **FTE-3** | **FTE-4** | **FTE-5** | **FTE-6** | **FTE-7** | **FTE-8** | **FTE-9** | **FTE-10** | **FTE-11** | **FTE-12** | **FTE-13** | **FTE-14** | **FTE-15** | **FTE-16** |
|---|---|---|---|---|---|---|---|---|---|---|---|---|---|---|---|---|
| Age | 59 | 50 | 70 | 74 | 70 | 56 | 49 | 41 | 41 | 71 | 71 | 71 | 72 | 71 | 72 | 71 |
| Pathology | NFTE | NFTE | NFTE | NFTE | NFTE | NFTE | NFTE | NFTE | NFTE | MTCO1[a] | MTCO1[a] | MTCO1[a] | MTCO1[a] | MTCO1[a] | MTCO1[a] | MTCO1[a] |
| Mol. prediction | NFTE | NFTE | NFTE | NFTE | NFTE | NFTE | NFTE | NFTE | NFTE | NFTE | NFTE | NFTE | NFTE | NFTE | NFTE | NFTE |
| Germline status | | | | | | | BRCA2 | BRCA2 | BRCA2 | | | | | | | |
| Concurrent cancer | NO | NO | NO | NO | NO | NO | NO | NO | NO | NO | NO | NO | NO | NO | NO | NO |
| **Specimen** | **FTE-18** | **FTE-19** | **FTE-37** | **FTE-25** | **FTE-28** | **FTE-29** | **FTE-30** | **FTE-31** | **FTE-32** | **FTE-33** | **FTE-34** | **FTE-35** | **FTE-36** | **FTE-26** | | |
| Age | 73 | 67 | 67 | 52 | 70 | 67 | 67 | 67 | 67 | 67 | 67 | 67 | 67 | 58 | | |
| Pathology | p53 sig | p53 sig | p53 sig | p53 sig | p53 sig | p53 sig | p53 sig | p53 sig | p53 sig | p53 sig | p53 sig | p53 sig | p53 sig | p53 sig | | |
| Mol. prediction | p53 sig | p53 sig | p53 sig | dSTIC | p53 sig | p53 sig | p53 sig | p53 sig | p53 sig | p53 sig | p53 sig | p53 sig | STIC | dSTIC | | |
| Germline status | | | | | | | | | | | | | | Lynch | | |
| Concurrent cancer | NO | NO | NO | NO | NO | YES | NO | NO | NO | NO | NO | NO | NO | NO | | |
| **Specimen** | **FTE-40** | **FTE-41** | **FTE-42** | **FTE-43** | **FTE-44** | **FTE-45** | **FTE-22** | **FTE-23** | **FTE-24** | **FTE-47** | **FTE-48** | **FTE-49** | **FTE-50** | **FTE-51** | **FTE-46** | |
| Age | 73 | 73 | NA | 72 | 58 | 58 | 72 | 60 | 73 | 66 | 72 | 55 | 44 | 68 | 51 | |
| Pathology | dSTIC | dSTIC | dSTIC | dSTIC | dSTIC | dSTIC | dSTIC | dSTIC | dSTIC | dSTIC | dSTIC | dSTIC | dSTIC | dSTIC | dSTIC | |
| Mol. prediction | dSTIC | dSTIC | dSTIC | dSTIC | dSTIC | dSTIC | dSTIC | dSTIC | dSTIC | STIC | STIC | STIC | STIC | STIC | p53 sig | |
| Germline status | | | | | Lynch | Lynch | | | BRCA1 | | | | VUS-1 | | | |
| Concurrent cancer | NO | NO | NA | NO | NO | NO | NO | YES | NO | NO | NO | NO | NO | NO | NO | |
| **Specimen** | **FTE-52** | **FTE-53** | **FTE-54** | **FTE-55** | **FTE-56** | **FTE-57** | **FTE-58** | **FTE-59** | **FTE-60** | **FTE-61** | **FTE-62** | **FTE-63** | **FTE-64** | **FTE-65** | **FTE-66** | |
| Age | 65 | 41 | 59 | 41 | 69 | 50 | 62 | 85 | 65 | 65 | 67 | 75 | 67 | 62 | 46 | |
| Pathology | STIC | STIC | STIC | STIC | STIC | STIC | STIC | STIC | STIC | STIC | STIC | STIC | STIC | STIC | STIC | |
| Mol. prediction | dSTIC | STIC | dSTIC | dSTIC | STIC | STIC | STIC | STIC | STIC | STIC | STIC | STIC | STIC | STIC | STIC | |
| Germline status | VUS-2 | BRCA2 | | BRCA2 | | | | | VUS-2 | VUS-2 | | | | BRCA1 | BRCA1 | |
| Concurrent cancer | NO | YES | NO | NO | YES | NO | YES | YES | NO | NO | NO | YES | YES | YES | NO | |
| **Specimen** | **FTE-67** | **FTE-68** | **FTE-69** | **FTE-70** | **FTE-71** | **FTE-20** | **FTE-17** | | | | | | | | | |
| Age | 46 | 49 | 66 | 41 | 44 | 70 | 73 | | | | | | | | | |
| Pathology | STIC | STIC | STIC | STIC | STIC | STIC | STIC | | | | | | | | | |
| Mol. prediction | STIC | STIC | STIC | STIC | STIC | STIC | dSTIC | | | | | | | | | |
| Germline status | BRCA1 | BRCA2 | BRCA2 | BRCA2 | VUS-1 | | | | | | | | | | | |
| Concurrent cancer | NO | NO | NO | YES | NO | NO | NO | | | | | | | | | |

Note: VUS-1: ATM(p.V455M), RAD50(p.R1260H); VUS-2: AIP, HOXB13.
[a]MT-CO1 loss regions.

**Table 4.** Correlations between molecular prediction and pathology diagnosis in the validation set.

| Specimen | FTE-72 | FTE-73 | FTE-74 | FTE-75 | FTE-76 | FTE-77 | FTE-78 | FTE-79 | FTE-80 | FTE-81 | FTE-82 | FTE-83 | FTE-84 | FTE-85 | FTE-86 |
|---|---|---|---|---|---|---|---|---|---|---|---|---|---|---|---|
| Age | 44 | 83 | 83 | 83 | 76 | 76 | 32 | 65 | 57 | 84 | 60 | 60 | 58 | 58 | 58 |
| Pathology | NFTE | NFTE | NFTE | NFTE | NFTE | NFTE | NFTE | NFTE | NFTE | NFTE | MTCO1[a] | MTCO1[a] | MTCO1[a] | MTCO1[a] | MTCO1[a] |
| Mol. prediction | NFTE | NFTE | NFTE | NFTE | NFTE | NFTE | NFTE | NFTE | NFTE | NFTE | NFTE | p53 sig | NFTE | NFTE | NFTE |
| Germline status | BRCA2 | | | | | | | | | | | | BRCA | BRCA | BRCA |
| Concurrent cancer | NO | NO | NO | NO | NO | NO | YES | YES | YES | YES | NO | NO | NO | NO | NO |
| **Specimen** | **FTE-87** | **FTE-88** | **FTE-89** | **FTE-90** | **FTE-91** | **FTE-92** | **FTE-93** | **FTE-94** | **FTE-95** | **FTE-147** | **FTE-148** | **FTE-149** | **FTE-150** | **FTE-151** | **FTE-152** |
| Age | 58 | 59 | 59 | 69 | 59 | 59 | 69 | 69 | 53 | 54 | 54 | 54 | 54 | 54 | 54 |
| Pathology | MTCO1[a] | MTCO1[a] | MTCO1[a] | MTCO1[a] | MTCO1[a] | MTCO1[a] | MTCO1[a] | MTCO1[a] | NFTE | p53 sig | p53 sig | p53 sig | p53 sig | p53 sig | p53 sig |
| Mol. prediction | NFTE | NFTE | NFTE | NFTE | NFTE | NFTE | NFTE | NFTE | NFTE | p53 sig | p53 sig | p53 sig | p53 sig | p53 sig | p53 sig |
| Germline status | BRCA | BRCA | BRCA | BRCA | BRCA | BRCA | BRCA | BRCA | | VUS-3 | VUS-3 | VUS-3 | VUS-3 | VUS-3 | VUS-3 |
| Concurrent cancer | NO | NO | NO | NO | NO | NO | NO | NO | NO | NO | NO | NO | NO | NO | NO |
| **Specimen** | **FTE-153** | **FTE-154** | **FTE-155** | **FTE-156** | **FTE-97** | **FTE-157** | **FTE-98** | **FTE-99** | **FTE-100** | **FTE-101** | **FTE-102** | **FTE-103** | **FTE-104** | **FTE-105** | **FTE-106** |
| Age | 54 | 54 | 54 | 56 | 56 | 56 | 56 | 56 | 71 | 72 | 58 | 58 | 40 | 58 | 69 |
| Pathology | p53 sig | p53 sig | p53 sig | p53 sig | p53 sig | dSTIC | dSTIC | dSTIC | dSTIC | STIC | STIC | STIC | STIC | STIC | STIC |
| Mol. prediction | p53 sig | p53 sig | p53 sig | dSTIC | p53 sig | p53 sig | dSTIC | dSTIC | dSTIC | STIC | STIC | STIC | p53 sig | STIC | STIC |
| Germline status | VUS-3 | VUS-3 | VUS-3 | BRCA1 | | BRCA1 | | | | | | | | | |
| Concurrent cancer | NO | NO | NO | NO | NO | NO | NO | NO | YES | YES | YES | YES | NO | YES | YES |
| **Specimen** | **FTE-107** | **FTE-108** | **FTE-109** | **FTE-110** | **FTE-111** | **FTE-112** | **FTE-113** | **FTE-114** | **FTE-115** | **FTE-116** | **FTE-117** | **FTE-118** | **FTE-119** | **FTE-120** | **FTE-121** |
| Age | 67 | 50 | 44 | 72 | 58 | 71 | 71 | 71 | 60 | 32 | 65 | 65 | 68 | 48 | 46 |
| Pathology | STIC | STIC | STIC | STIC | STIC | STIC | STIC | STIC | STIC | STIC | STIC | STIC | STIC | STIC | STIC |
| Mol. prediction | STIC | dSTIC | STIC | STIC | STIC | STIC | STIC | STIC | STIC | STIC | STIC | STIC | STIC | STIC | STIC |
| Germline status | | | BRCA2 | | | | | | BRCA1 | | | | | BRCA1 | |
| Concurrent cancer | YES | NO | NO | YES | YES | YES | YES | YES | NO | YES | YES | YES | YES | YES | YES |
| Specimen | **FTE-122** | **FTE-123** | **FTE-124** | **FTE-126** | **FTE-127** | **FTE-128** | **FTE-129** | **FTE-130** | **FTE-131** | **FTE-132** | **FTE-133** | **FTE-134** | **FTE-135** | **FTE-136** | **FTE-138** |
| Age | 57 | 57 | 57 | 59 | 59 | 34 | 68 | 68 | 68 | 68 | 53 | 32 | 65 | 48 | 59 |
| Pathology | STIC | STIC | STIC | STIC | STIC | STIC | STIC | STIC | STIC | STIC | STIC | HGSC | HGSC | HGSC | HGSC |
| Mol. prediction | STIC | STIC | STIC | STIC | STIC | STIC | STIC | STIC | STIC | STIC | STIC | STIC | STIC | STIC | STIC |
| Germline status | | | | VUS-4 | VUS-4 | BRCA1 | RAD51C | RAD51C | RAD51C | RAD51C | | | | BRCA1 | VUS-4 |
| Concurrent cancer | YES | YES | YES | YES | YES | YES | YES | YES | YES | YES | NO | YES | YES | YES | YES |
| **Specimen** | **FTE-139** | **FTE-140** | **FTE-141** | **FTE-142** | **FTE-143** | **FTE-144** | **FTE-145** | **FTE-125** | | | | | | | |
| Age | 34 | 67 | 62 | 62 | 69 | 72 | 67 | 84 | | | | | | | |
| Pathology | HGSC | HGSC | HGSC | HGSC | HGSC | HGSC | HGSC | HGSC | | | | | | | |
| Mol. prediction | STIC | STIC | STIC | STIC | STIC | STIC | STIC | STIC | | | | | | | |
| Germline status | BRCA1 | | BRCA1 | | | | | | | | | | | | |
| Concurrent cancer | YES | YES | YES | YES | YES | YES | YES | YES | | | | | | | |

Note: VUS-3: TP53; VUS-4: BRCA2, MLH1.
[a]MT-CO1 loss region.

among pathologists because of their minuscule sizes on the fallopian tube mucosa. In this study, we describe biological heterogeneity among STICs and elucidate the dependence of the origination of ovarian HGSC on a specific aneuploidy landscape. Furthermore, we develop the REAL-FAST offering a molecular assay to assist the STIC diagnosis. There are several biological and clinical implications.

Our data show that morphologically similar STICs are molecularly and biologically distinct. Proliferation activity in STICs is positively associated with the degree of aneuploidy, specifically in certain chromosomal arms or loci. Amplification of several cancer drivers, including *CCNE1*, *MYC*, *REQL4*, *NACC1*, and *RSF-1*, occurred in proliferatively active STICs but not in dormant STICs or NFTEs, including p53 signatures, suggesting that copy-number gain in these genes may play a role in tumor initiation. On the other hand, the degree of aneuploidy and its pattern in active STICs are indistinguishable from those of HGSC, suggesting that proliferatively active STICs are likely the immediate precursor of HGSC but that additional molecular changes other than copy-number alterations are required for progression from STIC to HGSC.

We detected aneuploidy in several HU-FTE regions, especially those with *TP53* mutations, that is, p53 signatures. The p53 signatures shared the same chr17 arm loss with STICs, but this is the only abnormality detected in contrast with pronounced aneuploidy involving multiple chromosomal regions in STICs and HGSCs. Alongside *TP53*, several tumor suppressors, including *BRCA1*, *NF1*, and *HOXB*, are also located in chr17 (chr17q21, chr17q21.32, and chr17q11.2, respectively). Because 22 of 25 p53 signatures studied manifested loss of one entire chromosome 17, and all p53 signatures reported harbor *TP53* missense mutations (8, 43, 44), it appears that epithelial cells within p53 signatures may have an increased risk for developing into STICs. Specifically, these normal-appearing fallopian tube epithelial cells harbor the two hits on *TP53*, including a missense mutation in one allele and a deletion in the other. In non-*BRCA1* women, the p53 signature epithelium may, theoretically, be equivalent to the NFTE from a germline *BRCA1*-inactivating mutation because in either scenario, one intact *BRCA1* remains, the other being inactivated or deleted. In contrast, in *BRCA1* carriers, the p53 signature epithelium presumably has two hits in *TP53* and in *BRCA1* due to their somatic mutations in one chromosome and concurrent deletion of the other.

Thus, we propose that p53 signatures are genetically predisposed to neoplastic transformation in fallopian tubes with *BRCA1* deleterious germline mutations. This finding, together with the fact that *TP53* mutation is the earliest and essential event for HGSC development known so far, offers a possible explanation for why *BRCA1* germline mutations, as compared with *BRCA2* (located in chr13) germline mutations, are associated with higher risk and earlier onset of HGSC. Our results are consistent with a prior study reporting that 85.71% of *BRCA1*-associated HGSC have loss of heterozygosity of the entire chromosome 17 (45). Mathematical modeling and epidemiological studies suggest a prolonged period (several decades) for a p53 signature to progress to a STIC (3, 14, 46), but from that point onward, it only takes another 6–7 years for a STIC to progress to an invasive HGSC. Therefore, once the STIC lesions achieve the higher level of chromosomal instability, tumor progression accelerates in some of the STICs.

Our results support REAL-FAST as a highly reproducible molecular diagnostic tool. The aneuploidy-based algorithm classifies STICs into three groups (Path-2, Path-3, and Path-4). Path-2 STICs harbor chr19q amplification, and Path-3 STICs harbor chr8q amplification. Path-4 STICs harbor chr22q loss but no chr19q or 8q amplification. STICs in Path-2 exhibit higher proliferative activity than Path-3 and Path-4. Path-2 STICs also overexpress IGFBP2, a marker associated with tumor cell proliferation and invasion (29). By careful examination of the STICs, we show that Path-2 and Path-3 STICs are characterized by loosely cohesive growth with frequent detached individual or clusters of STIC cells on the lesion surface that can readily disseminate. Therefore, Path-2 and Path-3 STICs, as compared with Path-4, are considered "aggressive" and potentially associated with recurrent HGSC.

Path-2 STICs have several additional chromosomal arm changes that can also be found in the TCGA ovarian cancer dataset (40) and in our digital karyotyping data using affinity-purified HGSC cells (47), notably, amplification in loci harboring *CCNE1*. *CCNE1* copy-number gain/amplification is found in 22% of STICs using dual color FISH (48), and intense cyclin E nuclear staining is found in 77% of STICs (28, 49). Copy-number gains, including *NACC1* and *Rsf-1*, are also detected in HGSC (50–52). Overexpression of *Rsf-1* has been reported in STICs (28). Of interest is the fact that Rsf-1 protein was shown to co-immunoprecipitate with cyclin E1 (53), and the Rsf-1/cyclin E1 interaction is required for cyclin E1-mediated tumor-promoting phenotypes. Co-upregulation of both gene products was also reported in HGSCs (53). In contrast, Path-3 STICs have a different aneuploidy pattern with chr8q amplification harboring *MYC*, *REQL4*, *SOX17*, *MAPK15*, *FOXH1*, *SHARPIN*, and *HSF1*. Path-4 STICs have a characteristic chr22q loss (**Fig. 2**). It is possible that the level of aneuploidy or specific chromosomal arm gain or loss accounts for the proliferation and discohesive histological characteristics of STIC lesions. The above results provide the first molecular evidence in supporting the view that STICs are biologically and genetically heterogeneous (2).

From the translational perspective, REAL-FAST may provide a molecular diagnostic tool to detect STICs or occult carcinoma in fallopian tubes. The current standard-of-care in detecting STICs and microscopic cancers is solely based on examining surgically removed fallopian tubes. Because the lesions are grossly inconspicuous, fallopian tube tissues are randomly sectioned and a limited portion is sent for microscopic evaluation. We estimated that less than 0.5% of fallopian tissues are eventually examined by a pathologist in practice, leaving most tissue in paraffin blocks that are archived or discarded. Theoretically, those unexamined fallopian tube tissues may potentially contain STIC lesions and minuscule HGSC, creating a substantial false negativity in routine practice. This concern was validated in our previous study in which we were able to detect new STICs after flipping the tissue block and cutting additional sections (54). Thus, the current clinical practice precludes the exquisite sensitivity in determining STICs and incidental HGSC in at-risk women, who before now had to deal with uncertainty and ambiguity even though their tubes were removed and the pathology diagnosis was negative. REAL-FAST warrants further evaluation to determine its clinical utility in comprehensive diagnosis of STICs and occult carcinomas using the "tubal-brushing" technique and the Falloposcope to sample the lesions (55, 56).

The REAL-FAST assay can be helpful to potentially stratify STICs into different clinically relevant groups. At least three recent studies have analyzed the incidence of pelvic or peritoneal HGSC after incidental STIC diagnosis on the fallopian tubes. All found a time-dependent increase in HGSC incidence after removal of fallopian tubes following diagnosis of incidental STICs. The risk of developing peritoneal carcinomatosis is 10% and 28% at the 5- and 10-year follow-up, respectively (57–59). Therefore, from a clinical standpoint, STICs are not a monolithic group of lesions in that some progress to HGSC and some do not. Future studies are required to correlate HGSC risk with the STICs from Path-2, Path-3, and Path-4. This risk stratification should have significant implications, as women with

high-risk STICs may potentially benefit from further clinical management such as consideration of clinical staging to detect occult cancer, frequent surveillance using imaging modalities and serum CA-125, and liquid biopsy to detect tumor-released DNA, miRNA, and methylated DNA markers (60, 61).

The findings reported here show that aneuploidy occurs early in morphologically normal epithelium, and its level increases in a non-random fashion involving specific chromosomal arm gain and loss from p53 signatures to proliferatively active STICs. Whole chr17 loss potentially offers a mechanism to simultaneous inactivation of *TP53* and *BRCA1*, the two most relevant tumor suppressors in initiation of HGSC (62, 63). This study identifies distinct molecular groups of STICs that are associated with increased proliferation and detached growth of the lesions. Finally, the REAL-FAST promises a molecular test for diagnosing HGSC precursor lesions *ex vivo* and *in vivo*. It should be noted that this pilot study contains higher proportion of cases with germline *BRCA1/2* mutation(s) compared with its actual prevalence in the population. Further studies, including more cases with both wild-type and germline-mutated BRCA1/2, would be needed to optimize the REAL-FAST algorithm and make it generalizable.

## Authors' Disclosures

C. Douville reports personal fees from Exact Sciences and Belay Diagnostics during the conduct of the study, as well as personal fees from Belay Diagnostics and Exact Sciences outside the submitted work; C. Douville also reports a patent for RealSeqS pending, licensed, and with royalties paid from Exact Sciences. Y.-W. Chien reports grants from Breakthrough Cancer during the conduct of the study. B.G. Wang reports personal fees from Genetron Health US outside the submitted work. R. Drapkin reports personal fees and other support from Repare Therapeutics, as well as other support from VOC Health outside the submitted work. M.H. Chui reports personal fees from Verastem Oncology and Roche outside the submitted work. T. Numan reports personal fees from Springer Publishing, DLA Piper LLC, and Wolters Kluwer Publishing outside the submitted work. N. Papadopoulos reports grants from SPORE—Ie Ming, as well as other support from Exact Sciences during the conduct of the study; N. Papadopolous also reports other support from Haystack/Quest, Haystack, PGDx, CAGE, NeoPhore, ManaTBio, Vidium, and Thrive outside the submitted work, as well as a patent for SafeSeqS pending and with royalties paid from Exact Sciences. In addition, N. Papadopoulos reports relationships with Sysmex, PGDx, Thrive, Thermo Fisher Scientific, Exact, Quest, and other companies that have licensed technologies from Johns Hopkins University, on which N. Papadopoulos is an inventor; these licenses and relationships are associated with royalty payments to N. Papadopoulos, and the terms of these arrangements are being managed by Johns Hopkins University in accordance with its conflict of interest policies. I.-M. Shih reports grants from NIH/NCI outside the submitted work. No disclosures were reported by the other authors.

## Authors' Contributions

**Y. Wang:** Conceptualization, resources, data curation, formal analysis, validation, investigation, visualization, methodology, writing–original draft, writing–review and editing. **C. Douville:** Conceptualization, data curation, software, formal analysis, supervision, validation, investigation, visualization, methodology, writing–original draft, writing–review and editing. **Y.-W. Chien:** Resources, formal analysis, validation. **B.G. Wang:** Resources, writing–review and editing. **C.-L. Chen:** Writing–review and editing. **A. Pinto:** Writing–review and editing. **S.A. Smith:** Writing–review and editing. **R. Drapkin:** Writing–review and editing. **M.H. Chui:** Writing–review and editing. **T. Numan:** Resources, writing–review and editing. **R. Vang:** Resources, validation, investigation, writing–review and editing. **N. Papadopoulos:** Conceptualization, resources, formal analysis, supervision, validation, investigation, visualization, methodology, writing–original draft, project administration, writing–review and editing. **T.-L. Wang:** Conceptualization, resources, supervision, funding acquisition, investigation, methodology, project administration, writing–review and editing. **I.-M. Shih:** Conceptualization, resources, formal analysis, supervision, funding acquisition, validation, investigation, visualization, methodology, writing–original draft, project administration, writing–review and editing.

## Acknowledgments

The research in this study was supported by the Richard W. TeLinde Endowment from the Johns Hopkins University, the Breakthrough Cancer Foundation (BTC-IOC), DoD-CDMRP Grant Award W81XWH-22-1-0852 (R. Drapkin and T.-L. Wang), and the Honorable Tina Brozman Foundation.

The publication costs of this article were defrayed in part by the payment of publication fees. Therefore, and solely to indicate this fact, this article is hereby marked "advertisement" in accordance with 18 USC section 1734.

## Note

Supplementary data for this article are available at Clinical Cancer Research Online (http://clincancerres.aacrjournals.org/).

Received March 30, 2023; revised July 21, 2023; accepted November 27, 2023; published first December 4, 2023.

## References

1. Siegel RL, Miller KD, Fuchs HE, Jemal A. Cancer statistics, 2022. CA Cancer J Clin 2022;72:7–33.
2. Shih IM, Wang Y, Wang TL. The origin of ovarian cancer species and precancerous landscape. Am J Pathol 2021;191:26–39.
3. Wu RC, Wang P, Lin SF, Zhang M, Song Q, Chu T, et al. Genomic landscape and evolutionary trajectories of ovarian cancer precursor lesions. J Pathol 2019;248:41–50.
4. Pisanic TR II, Wang Y, Sun H, Considine M, Li L, Wang TH, et al. Methylomic landscapes of ovarian cancer precursor lesions. Clin Cancer Res 2020;26:6310–20.
5. Kroeger PT Jr, Drapkin R. Pathogenesis and heterogeneity of ovarian cancer. Curr Opin Obstet Gynecol 2017;29:26–34.
6. Vang R, Visvanathan K, Gross A, Maambo E, Gupta M, Kuhn E, et al. Validation of an algorithm for the diagnosis of serous tubal intraepithelial carcinoma. Int J Gyn Pathol 2012;31:243–53.
7. Vang R, Shih IM. Serous tubal intra-epithelial carcinoma: what do we really know at this point? Histopathology 2022;81:542–55.
8. Lee Y, Miron A, Drapkin R, Nucci MR, Medeiros F, Saleemuddin A, et al. A candidate precursor to serous carcinoma that originates in the distal fallopian tube. J Pathol 2007;211:26–35.
9. Lee Y, Medeiros F, Kindelberger D, Callahan MJ, Muto MG, Crum CP. Advances in the recognition of tubal intraepithelial carcinoma: applications to cancer screening and the pathogenesis of ovarian cancer. Adv Anat Pathol 2006;13:1–7.
10. Pisanic TR II, Cope LM, Lin SF, Yen TT, Athamanolap P, Asaka R, et al. Methylomic analysis of ovarian cancers identifies tumor-specific alterations readily detectable in early precursor lesions. Clin Cancer Res 2018;24:6536–47.
11. Wang Y, Li L, Douville C, Cohen JD, Yen TT, Kinde I, et al. Evaluation of liquid from the papanicolaou test and other liquid biopsies for the detection of endometrial and ovarian cancers. Sci Transl Med 2018;10:eaap8793.
12. Soong TR, Howitt BE, Miron A, Horowitz NS, Campbell F, Feltmate CM, et al. Evidence for lineage continuity between early serous proliferations (ESPs) in the fallopian tube and disseminated high-grade serous carcinomas. J Pathol 2018;246:344–51.
13. Eckert MA, Pan S, Hernandez KM, Loth RM, Andrade J, Volchenboum SL, et al. Genomics of ovarian cancer progression reveals diverse metastatic trajectories, including intraepithelial metastasis to the fallopian tube. Cancer Discov 2016;6:1342–51.
14. Labidi-Galy SI, Papp E, Hallberg D, Niknafs N, Adleff V, Noe M, et al. High grade serous ovarian carcinomas originate in the fallopian tube. Nat Commun 2017;8:1093.
15. Garraway LA, Lander ES. Lessons from the cancer genome. Cell 2013;153:17–37.
16. Shih IM, Zhou W, Goodman SN, Lengauer C, Kinzler KW, Vogelstein B. Evidence that genetic instability occurs at an early stage of colorectal tumorigenesis. Cancer Res 2001;61:818–22.
17. Kuhn E, Meeker A, Wang TL, Sehdev AS, Kurman RJ, Shih Ie M. Shortened telomeres in serous tubal intraepithelial carcinoma: an early event in ovarian high-grade serous carcinogenesis. Am J Surg Pathol 2010;34:829–36.
18. Amari M, Suzuki A, Moriya T, Yoshinaga K, Amano G, Sasano H, et al. LOH analyses of premalignant and malignant lesions of human breast: frequent LOH in 8p, 16q, and 17q in atypical ductal hyperplasia. Oncol Rep 1999;6:1277–80.

19. Newburger DE, Kashef-Haghighi D, Weng Z, Salari R, Sweeney RT, Brunner AL, et al. Genome evolution during progression to breast cancer. Genome Res 2013; 23:1097–108.
20. Ross-Innes CS, Becq J, Warren A, Cheetham RK, Northen H, O'Donovan M, et al. Whole-genome sequencing provides new insights into the clonal architecture of Barrett's esophagus and esophageal adenocarcinoma. Nat Genet 2015; 47:1038–46.
21. Stachler MD, Taylor-Weiner A, Peng S, McKenna A, Agoston AT, Odze RD, et al. Paired exome analysis of Barrett's esophagus and adenocarcinoma. Nat Genet 2015;47:1047–55.
22. Douville C, Cohen JD, Ptak J, Popoli M, Schaefer J, Silliman N, et al. Assessing aneuploidy with repetitive element sequencing. Proc Natl Acad Sci USA 2020; 117:4858–63.
23. Douville C, Springer S, Kinde I, Cohen JD, Hruban RH, Lennon AM, et al. Detection of aneuploidy in patients with cancer through amplification of long interspersed nucleotide elements (LINEs). Proc Natl Acad Sci USA 2018;115: 1871–6.
24. Zeki S, Graham TA, McDonald SA. Utilizing DNA mutations to trace epithelial cell lineages in human tissues. Methods Mol Biol 2012;916:289–301.
25. Greaves LC, Preston SL, Tadrous PJ, Taylor RW, Barron MJ, Oukrif D, et al. Mitochondrial DNA mutations are established in human colonic stem cells, and mutated clones expand by crypt fission. Proc Natl Acad Sci USA 2006;103:714–9.
26. Fellous TG, McDonald SA, Burkert J, Humphries A, Islam S, De-Alwis NM, et al. A methodological approach to tracing cell lineage in human epithelial tissues. Stem Cells 2009;27:1410–20.
27. Madan E, Palma AM, Vudatha V, Trevino JG, Natarajan KN, Winn RA, et al. Cell competition in carcinogenesis. Cancer Res 2022;82:4487–96.
28. Sehdev AS, Kurman RJ, Kuhn E, Shih Ie M. Serous tubal intraepithelial carcinoma upregulates markers associated with high-grade serous carcinomas including Rsf-1 (HBXAP), cyclin E and fatty acid synthase. Mod Pathol 2010;23: 844–55.
29. Wang Y, Huang P, Wang BG, Murdock T, Cope L, Hsu FC, et al. Spatial transcriptomic analysis of ovarian cancer precursors reveals reactivation of IGFBP2 during pathogenesis. Cancer Res 2022;82:4528–41.
30. Jung JG, Stoeck A, Guan B, Wu RC, Zhu H, Blackshaw S, et al. Notch3 interactome analysis identified WWP2 as a negative regulator of Notch3 signaling in ovarian cancer. PLoS Genet 2014;10:e1004751.
31. Song G, Chen L, Zhang B, Song Q, Yu Y, Moore C, et al. Proteome-wide tyrosine phosphorylation analysis reveals dysregulated signaling pathways in ovarian tumors. Mol Cell Proteomics 2019;18:448–60.
32. Olshen AB, Venkatraman ES, Lucito R, Wigler M. Circular binary segmentation for the analysis of array-based DNA copy number data. Biostatistics 2004;5: 557–72.
33. Yemelyanova A, Vang R, Kshirsagar M, Lu D, Marks MA, Shih Ie M, et al. Immunohistochemical staining patterns of p53 can serve as a surrogate marker for TP53 mutations in ovarian carcinoma: an immunohistochemical and nucleotide sequencing analysis. Mod Pathol 2011;24:1248–53.
34. Tjebbes GW, Leppers vd Straat FG, Tilanus MG, Hordijk GJ, Slootweg PJ. p53 tumor suppressor gene as a clonal marker in head and neck squamous cell carcinoma: p53 mutations in primary tumor and matched lymph node metastases. Oral Oncol 1999;35:384–9.
35. Kuhn E, Kurman RJ, Vang R, Sehdev AS, Han G, Soslow R, et al. TP53 mutations in serous tubal intraepithelial carcinoma and concurrent pelvic high-grade serous carcinoma- evidence supporting the clonal relationship of the two lesions. J Pathol 2012;226:421–6.
36. Ben-David U, Amon A. Context is everything: aneuploidy in cancer. Nat Rev Genet 2020;21:44–62.
37. O'Hagan RC, Chang S, Maser RS, Mohan R, Artandi SE, Chin L, et al. Telomere dysfunction provokes regional amplification and deletion in cancer genomes. Cancer Cell 2002;2:149–55.
38. Bach DH, Zhang W, Sood AK. Chromosomal instability in tumor initiation and development. Cancer Res 2019;79:3995–4002.
39. Nooteboom M, Johnson R, Taylor RW, Wright NA, Lightowlers RN, Kirkwood TB, et al. Age-associated mitochondrial DNA mutations lead to small but significant changes in cell proliferation and apoptosis in human colonic crypts. Aging Cell 2010;9:96–9.
40. Network Cgar. Integrated genomic analyses of ovarian carcinoma. Nature 2011; 474:609–15.
41. Visvanathan K, Vang R, Shaw P, Gross A, Soslow R, Parkash V, et al. Diagnosis of serous tubal intraepithelial carcinoma based on morphologic and immunohistochemical features: a reproducibility study. Am J Surg Pathol 2011;35:1766–75.
42. Carlson JW, Jarboe EA, Kindelberger D, Nucci MR, Hirsch MS, Crum CP. Serous tubal intraepithelial carcinoma: diagnostic reproducibility and its implications. Int J Gynecol Pathol 2010;29:310–4.
43. Crum CP, Drapkin R, Miron A, Ince TA, Muto M, Kindelberger DW, et al. The distal fallopian tube: a new model for pelvic serous carcinogenesis. Curr Opin Obstet Gynecol 2007;19:3–9.
44. Folkins AK, Jarboe EA, Saleemuddin A, Lee Y, Callahan MJ, Drapkin R, et al. A candidate precursor to pelvic serous cancer (p53 signature) and its prevalence in ovaries and fallopian tubes from women with BRCA mutations. Gynecol Oncol 2008;109:168–73.
45. Chisholm KM, Goff BA, Garcia R, King MC, Swisher EM. Genomic structure of chromosome 17 deletions in BRCA1-associated ovarian cancers. Cancer Genet Cytogenet 2008;183:41–8.
46. Wu NY, Fang C, Huang HS, Wang J, Chu TY. Natural history of ovarian high-grade serous carcinoma from time effects of ovulation inhibition and progesterone clearance of p53-defective lesions. Mod Pathol 2020;33:29–37.
47. Nakayama K, Nakayama N, Jinawath N, Salani R, Kurman RJ, Shih Ie M, et al. Amplicon profiles in ovarian serous carcinomas. Int J Cancer 2007;120:2613–7.
48. Kuhn E, Wang TL, Doberstein K, Bahadirli-Talbott A, Ayhan A, Sehdev AS, et al. CCNE1 amplification and centrosome number abnormality in serous tubal intraepithelial carcinoma: further evidence supporting its role as a precursor of ovarian high-grade serous carcinoma. Mod Pathol 2016;29:1254–61.
49. Karst AM, Jones PM, Vena N, Ligon AH, Liu JF, Hirsch MS, et al. Cyclin E1 deregulation occurs early in secretory cell transformation to promote formation of fallopian tube-derived high-grade serous ovarian cancers. Cancer Res 2014;74: 1141–52.
50. Shih Ie M, Nakayama K, Wu G, Nakayama N, Zhang J, Wang TL. Amplification of the ch19p13.2 NACC1 locus in ovarian high-grade serous carcinoma. Mod Pathol 2011;24:638–45.
51. Nakayama K, Nakayama N, Davidson B, Sheu JJ, Jinawath N, Santillan A, et al. A BTB/POZ protein, NAC-1, is related to tumor recurrence and is essential for tumor growth and survival. Proc Natl Acad Sci USA 2006;103:18739–44.
52. Shih I-M, Sheu JJ, Santillan A, Nakayama K, Yen MJ, Bristow RE, et al. Amplification of a chromatin remodeling gene, Rsf-1/HBXAP, in ovarian carcinoma. Proc Natl Acad Sci USA 2005;102:14004–9.
53. Sheu JJ, Choi JH, Guan B, Tsai FJ, Hua CH, Lai MT, et al. Rsf-1, a chromatin remodelling protein, interacts with cyclin E1 and promotes tumour development. J Pathol 2013;229:559–68.
54. Visvanathan K, Shaw P, May BJ, Bahadirli-Talbott A, Kaushiva A, Risch H, et al. Fallopian tube lesions in women at high risk for ovarian cancer: a multicenter study. Cancer Prev Res 2018;11:697–706.
55. Chui MH, Vang R, Wang TL, Shih IM, VandenBussche CJ. Cytomorphologic and molecular analyses of fallopian tube fimbrial brushings for diagnosis of serous tubal intraepithelial carcinoma. Cancer Cytopathol 2019;127:192–201.
56. Cordova R, Kiekens K, Burrell S, Drake W, Kmeid Z, Rice P, et al. Sub-millimeter endoscope demonstrates feasibility of *in vivo* reflectance imaging, fluorescence imaging, and cell collection in the fallopian tubes. J Biomed Opt 2021;26:076001.
57. Steenbeek MP, van Bommel MHD, Bulten J, Hulsmann JA, Bogaerts J, Garcia C, et al. Risk of peritoneal carcinomatosis after risk-reducing salpingo-oophorectomy: a systematic review and individual patient data meta-analysis. J Clin Oncol 2022;40:1879–91.
58. Linz VC, Lowe A, van der Ven J, Hasenburg A, Battista MJ. Incidence of pelvic high-grade serous carcinoma after isolated STIC diagnosis: a systematic review of the literature. Front Oncol 2022;12:951292.
59. Ruel-Laliberte J, Kasasni SM, Oprea D, Viau M. Outcome and management of serous tubal intraepithelial carcinoma following opportunistic salpingectomy: systematic review and meta-analysis. J Obstet Gynaecol Can 2022;44:1174–80.
60. Liberto JM, Chen SY, Shih IM, Wang TH, Wang TL, Pisanic TR II. Current and emerging methods for ovarian cancer screening and diagnostics: a comprehensive review. Cancers 2022;14:2885.
61. Krimmel JD, Schmitt MW, Harrell MI, Agnew KJ, Kennedy SR, Emond MJ, et al. Ultra-deep sequencing detects ovarian cancer cells in peritoneal fluid and reveals somatic TP53 mutations in noncancerous tissues. Proc Natl Acad Sci USA 2016; 113:6005–10.
62. George SH, Shaw P. BRCA and early events in the development of serous ovarian cancer. Front Oncol 2014;4:5.
63. Norquist BM, Brady MF, Harrell MI, Walsh T, Lee MK, Gulsuner S, et al. Mutations in homologous recombination genes and outcomes in ovarian carcinoma patients in GOG 218: an NRG oncology/gynecologic oncology group study. Clin Cancer Res 2018;24:777–83.